





RESEARCH ARTICLE | JULY 15 2025

# Determination of deformation potentials in InGaN at visible light region

Keito Mori-Tamamura  ; Atsushi A. Yamaguchi  ; Shuhei Ichikawa  ; Kazunobu Kojima *J. Appl. Phys.* 138, 035701 (2025)<https://doi.org/10.1063/5.0276104>

## Articles You May Be Interested In

High-color-rendering-index phosphor-free InGaN-based white light-emitting diodes by carrier injection enhancement via V-pits

*Appl. Phys. Lett.* (October 2020)

Optical polarization characteristics of *c*-plane InGaN/GaN asymmetric nanostructures

*J. Appl. Phys.* (December 2015)

A simple theoretical approach to analyze polarization properties in semipolar and nonpolar InGaN quantum wells

*Appl. Phys. Lett.* (March 2011)

21 July 2025 08:35:50

# Determination of deformation potentials in InGaN at visible light region

Cite as: J. Appl. Phys. 138, 035701 (2025); doi: 10.1063/5.0276104

Submitted: 16 April 2025 · Accepted: 26 June 2025 ·

Published Online: 15 July 2025



Keito Mori-Tamamura,<sup>1,a)</sup> Atsushi A. Yamaguchi,<sup>2</sup> Shuhei Ichikawa,<sup>1</sup> and Kazunobu Kojima<sup>1</sup>

## AFFILIATIONS

<sup>1</sup>Division of Electrical, Electronic and Infocommunications Engineering, Graduate School of Engineering, Osaka University, Suita, Osaka 565-0871, Japan

<sup>2</sup>Department of Electrical and Electronic Engineering, Graduate School of Engineering, Kanazawa Institute of Technology, Nonoichi, Ishikawa 921-8501, Japan

<sup>a)</sup>Author to whom correspondence should be addressed: [mori@sfm.eei.eng.osaka-u.ac.jp](mailto:mori@sfm.eei.eng.osaka-u.ac.jp)

## ABSTRACT

We determined deformation potentials in  $\text{In}_x\text{Ga}_{1-x}\text{N}$  at visible light-emitting region ( $0 \leq x \leq 0.4$ ) by analysis based on the  $\mathbf{k} \cdot \mathbf{p}$  perturbation theory for numerous experimental data of energy separation between the two valence bands ( $\Delta E$ ) in InGaN quantum wells with various InN mole fractions and substrate orientations. The deformation potentials for InGaN were obtained by linear interpolation between the values of InN in this study and the accurate reported values of GaN, and the deformation potentials for InN, applicable to InGaN with InN mole fraction ranging from 0 to 0.4, were obtained as  $D_3 = 2.55$  eV,  $D_4 = -10.9$  eV,  $D_5 = -0.21$  eV, and  $D_6 = -13.0$  eV.

© 2025 Author(s). All article content, except where otherwise noted, is licensed under a Creative Commons Attribution (CC BY) license (<https://creativecommons.org/licenses/by/4.0/>). <https://doi.org/10.1063/5.0276104>

## I. INTRODUCTION

InGaN quantum wells (QWs) are attractive materials as active layers for light-emitting diodes (LEDs) and laser diodes (LDs) because they can emit light with colors ranging from near ultraviolet to near infrared by controlling the alloy fraction. Taking advantage of this characteristic, progress is being made in commercializing InGaN-QW-based monolithic micro-LEDs with the emission of three primary colors. However, although InGaN-based blue and green LEDs have high external quantum efficiency value (80% and 50%, respectively),<sup>1,2</sup> the values of red LEDs are still low (4–10%).<sup>3,4</sup> Generally, InGaN-QWs are in-plane compressive strain systems since lattice mismatch between the InGaN-QW layer and the underlying GaN layer. Therefore, a large piezoelectric field is generated in the QW, and the field causes separation of electron and hole wavefunctions, which reduces the radiative recombination rate.<sup>5–7</sup> InGaN-QWs, which are typically fabricated on the *c*-plane GaN and sapphire substrates, are greatly affected by this effect of reducing radiative rate. Additionally, this effect is more pronounced with increasing InN mole fraction due to the larger in-plane strain.<sup>8–10</sup> To circumvent this issue, nonpolar and semipolar plane InGaN-QW structures have been fabricated, which have a higher

radiative recombination rate compared with *c*-plane QWs.<sup>11–13</sup> The emission from non-*c*-plane QWs has optical anisotropy because of the breaking of sixfold symmetry. In addition, the optical polarization direction is known to depend on the InN mole fraction and substrate orientation.<sup>14,15</sup> For example, in an RGB-micro-LED monolithically fabricated on a semipolar substrate, it is desirable for the polarization directions of the blue-, green-, and red-light emission to be aligned. On the other hand, in a semipolar plane LD, it is desirable for utilizing the cleaver plane as a cavity mirror. Therefore, understanding the optical polarization property of InGaN-QWs is very important. Before discussing the polarization property of InGaN-QWs, a schematic diagram of a band structure and a coordinate system ( $X'$ ,  $Y'$ ,  $Z'$ ) used in this study are defined as shown in Fig. 1. The  $X'$ -axis is the direction perpendicular to the *c*-axis, the  $Y'$ -axis is the projection direction of the *c*-axis, and the  $Z'$ -axis is the normal direction to the substrate plane. The parameter  $\theta$  is the orientation angle between the *c*-axis and the  $Z'$ -axis. The polarization characteristics of InGaN-QWs are mainly dominated by wavefunction property of the topmost valence band (A-band). Two bands near the top of the valence band (A- and B-bands) of InGaN-QW are close in energy and have different characters of wavefunction ( $|X'\rangle$ -like or  $|Y'\rangle$ -like). Hence, the

21 July 2025 08:35:50

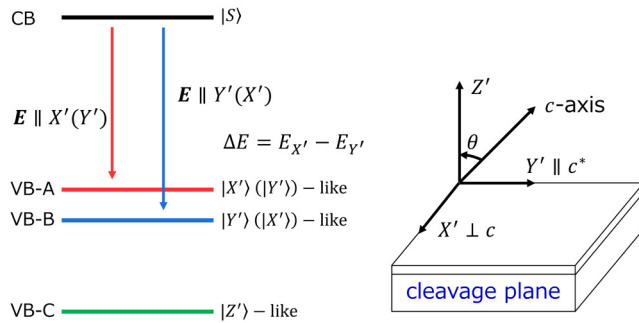


**FIG. 1.** A schematic diagram of the band structure and the coordinate system in InGaN-QWs.  $E$ : optical polarization,  $|S\rangle$ : wavefunction of s-orbital derived from group-III elements, and  $|X'\rangle$ ,  $|Y'\rangle$ ,  $|Z'\rangle$ : wavefunction of p-orbital derived from nitrogen. The  $X'$ -axis is the direction perpendicular to the  $c$ -axis, the  $Y'$ -axis is the projection direction of the  $c$ -axis, and the  $Z'$ -axis is the normal direction to the substrate plane. The parameter  $\theta$  is the orientation angle between the  $c$ -axis and the  $Z'$ -axis.

energy difference ( $\Delta E$ ) between the band whose wavefunction has  $|X'\rangle$ -like and  $|Y'\rangle$ -like properties is an important parameter that determines the optical polarization property. When  $\Delta E$  is a positive value, this means that the wavefunction of A-band has the  $|X'\rangle$ -like character, and the emission is polarized in the  $X'$ -direction. In contrast, when  $\Delta E$  is a negative value, this means that the wavefunction of A-band has the  $|Y'\rangle$ -like character, and the cleavage plane can be used as cavity mirrors for LDs.

According to the  $\mathbf{k} \cdot \mathbf{p}$  perturbation theory,<sup>16</sup> the optical polarization property of InGaN-QWs is mainly dependent on the deformation potentials.<sup>14,15</sup> The value of deformation potentials of InGaN are usually estimated by linear interpolation between those of GaN and InN. In the previous report, all accurate deformation potentials for GaN were experimentally determined from reflectance spectroscopy.<sup>17</sup> However, although many deformation potentials of InN obtained by experiments<sup>14,18–21</sup> and first-principles calculations<sup>22–27</sup> have been reported, these values are very scattered (Table I) and still unreliable. Figure 2 shows a comparison between experimental data<sup>14,28–30</sup> and theoretical calculation results that used reported deformation potentials in InGaN, for energy separation between the two valence bands  $\Delta E$  of the (11 $\bar{2}2$ )-plane InGaN-QW on GaN substrates with various InN mole fractions. Theoretical calculations were performed based on the  $\mathbf{k} \cdot \mathbf{p}$  theory, and the reported values of deformation potentials in InGaN were obtained by linear interpolation of the accurate values of GaN<sup>17</sup> and the reported values of InN.<sup>14,19–24,26</sup> As shown in Fig. 2, many of the theoretical curves cannot reproduce the experimental results. The curve E is the only one that reproduces the experimental data. However, this reported value is based on the reference value that has three degrees of freedom<sup>20</sup> ( $D_3$ – $D_6$  can be freely combined). Thus, it is still difficult to say that accurate values of deformation potentials in InGaN have been obtained.

In this work, we derived the accurate value of deformation potentials in InGaN with no degrees of freedom, which reproduce experimental data in InGaN-QWs with various InN mole fractions and substrate orientations, by theoretical analysis based on the

**TABLE I.** Reported deformation potentials  $D_i$  for InN in units of eV.  $D_1$  and  $D_2$  are omitted because they do not affect optical anisotropy.

	InN	$D_3$	$D_4$	$D_5$	$D_6$
Experiment					
A	Ueda <i>et al.</i> <sup>14</sup>	0.1	−0.05	−3.5	−8.8
B	Gil <i>et al.</i> <sup>18</sup>	5.06	−2.53		
C	Scheibenzuber <i>et al.</i> <sup>19</sup>	5.06	−2.53	−3.5	−7.2
D	Tamaki <i>et al.</i> <sup>20</sup>	2.4	−6.3	−1.2	−9.8 <sup>a</sup>
E	Sakai <i>et al.</i> <sup>21</sup>	2.4	−6.3	−1.2	−12.3
First-principles calculation					
F	Vurgaftman <i>et al.</i> <sup>22</sup>	8.2	−4.1	−4.0	−5.5
G	Vurgaftman <i>et al.</i> <sup>23</sup>	5.2	−2.7	−2.6	−4.3
H	Yan <i>et al.</i> <sup>24</sup>	2.68	−1.78	−2.07	−3.02
I	Łepkowski <i>et al.</i> <sup>25</sup>	2.7	−1.51	−2.55	
J	Ziembivki <i>et al.</i> <sup>26</sup>	3.29	−1.85	−1.25	−2.27
K	Luo <i>et al.</i> <sup>27</sup>	3.96	−0.52	−2.32	

<sup>a</sup>Obtained by private communication.

$6 \times 6 \mathbf{k} \cdot \mathbf{p}$  perturbation theory. In addition, we theoretically proposed the structure of three primary color emitting InGaN-QWs with matched polarization directions and the structure of InGaN-QW-based LDs that can use cleaved planes as cavity mirrors.

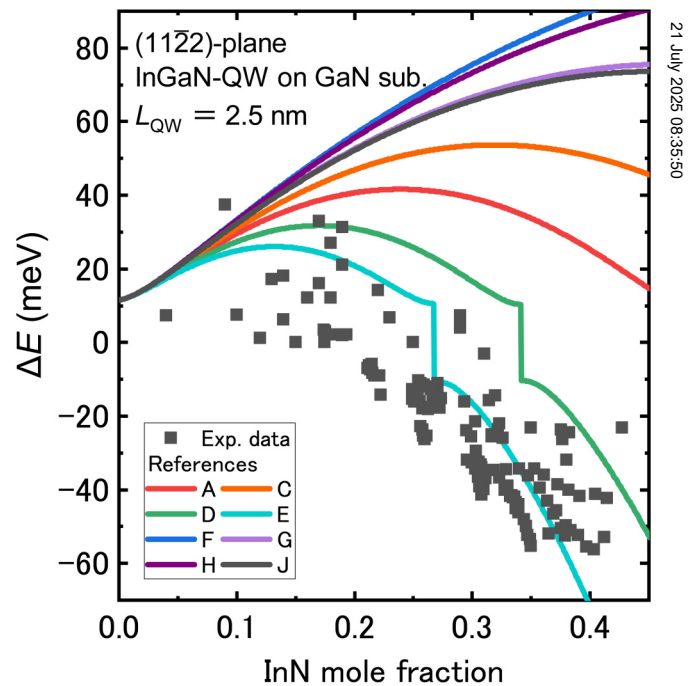


**FIG. 2.** A comparison between experimental data<sup>14,28–30</sup> and theoretical calculation results used reported deformation potentials in InGaN,<sup>14,19–24,26</sup> for energy separation  $\Delta E$  of (11 $\bar{2}2$ )-plane InGaN-QWs with various InN mole fractions. Alphabet labels in the figure correspond to the symbols in Table I.

## II. DETERMINATION OF DEFORMATION POTENTIALS

First, we explain by using an analytical equation based on the  $\mathbf{k} \cdot \mathbf{p}$  theory how the energy separation in InGaN-QWs occurs. The

analytical expression for energy separation ( $\Delta E$ ) in InGaN-QWs with arbitrary InN mole fraction and crystal orientation is as follows:<sup>15</sup>

$$\Delta E = \frac{(3D_4 + D_5)(\varepsilon_a - \varepsilon_c)}{2} \sin^2 \theta - \varepsilon_{\parallel} \left( 1 + \frac{2c_{12}}{c_{11}} \right) \sin^2 \theta \left[ \left( D_4 - D_5 - \frac{D_3 + 2D_4}{1 + 2c_{12}/c_{11}} \right) + (D_3 - D_4 - D_5 + 2\sqrt{2}D_6) \cos^2 \theta \right] + \frac{\hbar^2}{2m_0} \left( \frac{\pi}{L_{\text{QW}}} \right)^2 \sin^2 \theta \left[ (A_4 - A_5) + (A_3 - A_4 - A_5 + 2\sqrt{2}A_6) \cos^2 \theta \right], \quad (1)$$

where  $\theta$  is the crystal orientation;  $\hbar$  is the Dirac constant;  $m_0$  is the electron rest mass;  $L_{\text{QW}}$  is the QW width;  $A_i$ ,  $D_i$ , and  $c_{ij}$  are the valence band effective mass parameters, the deformation potentials, and the elastic constants in  $\text{In}_x\text{Ga}_{1-x}\text{N}$  ( $x$ : In composition), respectively; and  $\varepsilon_{a,c,\parallel}$  are the  $a$ - and  $c$ -axes strain, and average of the in-plane anisotropic strain in InGaN-QWs, respectively. Note that Eq. (1) is derived as the infinite barrier QW approximation neglecting crystal-field splitting, spin-orbit interaction, and internal electric fields, in order to express analytically. In this equation, the first, second, and third terms are expressed as the energy separation by the anisotropic effects of in-plane strain, deformation potentials, and valence band effective masses, respectively. The third term expresses the QW effect, which depends on the QW width  $L_{\text{QW}}$ . The reported  $\Delta E$  values of semipolar InGaN-QWs show that  $\Delta E$  values do not change with QW width.<sup>14,31</sup> Hence, the impact of valence band anisotropic effective masses (QW) effect on the energy separation is very small, and the  $\Delta E$  values mainly depend on the deformation potentials. Therefore, the more plausible valence band effective mass parameters  $A_i$  set is one in which the calculation results in a small absolute value of  $\Delta E$  with almost no change in optical polarization degree ( $\Delta E$ ) with respect to the QW width. In calculations using several valence band effective mass parameters sets of GaN and InN reported so far,<sup>22,23,26,32–34</sup> that in Ref. 23 was closest to the above conditions. Thus, we used the values from Ref. 23 as valence band effective mass parameters set for GaN and InN.

Generally, deformation potentials in semiconductors were experimentally determined from reflectance spectroscopy at cryogenic temperature.<sup>17,35,36</sup> However, three exciton peaks of A-, B-, and C-bands are not observed in reflectance spectra<sup>37</sup> since crystal quality of InN is still low. Thus, determination of deformation potentials is difficult by the reflectance spectroscopy method. Therefore, in this study, we assumed that the values of deformation potentials in  $\text{In}_x\text{Ga}_{1-x}\text{N}$  at the visible light-emitting region ( $0 \leq x \leq 0.4$ ) can be obtained by linear interpolation between the values of GaN and InN and determined the values of InN that reproduce the experimental  $\Delta E$  values in InGaN-QWs with various InN mole fractions and substrate orientations, while fixing the accurate values of GaN.<sup>17</sup> Note that it is uncertain that material parameters of alloy semiconductors are proportionally distributed with respect to the alloy composition. In previous study, the deformation potential  $D_5$  of InGaN was experimentally determined.<sup>38</sup> In Fig. 6 in Ref. 38, it can be said that the deformation potential  $D_5$  is proportional to In composition at low In composition region ( $0 \leq x \leq 0.2$ ).

Furthermore, in previous studies, the authors assumed that the deformation potentials of InGaN could be obtained through linear interpolation between the values of GaN and InN.<sup>14,19–24,26,27</sup> Therefore, we assumed that linear interpolation in order to compare under the same condition.

The valence band structure in the InGaN-QWs is expressed as follows based on the  $\mathbf{k} \cdot \mathbf{p}$  theory:<sup>16</sup>

$$\mathbf{H} = \begin{pmatrix} F & -K^* & -H^* & 0 & 0 & 0 \\ -K & G & H & 0 & 0 & \Delta \\ -H & H^* & \lambda & 0 & \Delta & 0 \\ 0 & 0 & 0 & F & -K & H \\ 0 & 0 & \Delta & -K^* & G & -H^* \\ 0 & \Delta & 0 & H^* & -H & \lambda \end{pmatrix} \begin{pmatrix} |u_1\rangle \\ |u_2\rangle \\ |u_3\rangle \\ |u_4\rangle \\ |u_5\rangle \\ |u_6\rangle \end{pmatrix}, \quad (2)$$

where

$$|u_{1,4}\rangle = \mp 1/\sqrt{2} [X \pm iY], \uparrow\downarrow,$$

$$|u_{2,5}\rangle = \pm 1/\sqrt{2} [X \mp iY], \uparrow\downarrow,$$

$$|u_{3,6}\rangle = |Z, \uparrow\downarrow\rangle,$$

$$F = \Delta_1 + \Delta_2 + \lambda + \theta, G = \Delta_1 - \Delta_2 + \lambda + \theta,$$

$$\lambda = \frac{\hbar^2}{2m_0} \left[ A_1 k_z^2 + A_2 (k_x^2 + k_y^2) \right] + D_1 \varepsilon_{zz} + D_2 (\varepsilon_{xx} + \varepsilon_{yy}),$$

$$\theta = \frac{\hbar^2}{2m_0} \left[ A_3 k_z^2 + A_4 (k_x^2 + k_y^2) \right] + D_3 \varepsilon_{zz} + D_4 (\varepsilon_{xx} + \varepsilon_{yy}),$$

$$K = \frac{\hbar^2}{2m_0} A_5 (k_x + ik_y)^2 + D_5 (\varepsilon_{xx} - \varepsilon_{yy} + i\varepsilon_{xy}),$$

$$H = \frac{\hbar^2}{2m_0} A_6 k_z (k_x + ik_y) + D_6 (\varepsilon_{zx} + i\varepsilon_{yz}), \Delta = \sqrt{2}\Delta_3,$$

where  $|u_1\rangle, |u_2\rangle, |u_3\rangle, \dots, |u_6\rangle$  are bases of the wavefunctions;  $|X\rangle, |Y\rangle$ , and  $|Z\rangle$  are the atomic wavefunctions of  $p$ -orbital derived from nitrogen;  $k_{x,y,z}$  are the wavenumber;  $\varepsilon_{ij}$  are the strain; and the others are shown in Table II. The material parameters of InGaN were provided by linear interpolation between material parameters of GaN and those of InN. The strain induced in the InGaN-QW layer was assumed to be in-plane compressive lattice strain with the

**TABLE II.** The material parameters for theoretical calculation in this study. The parameters of InGaN were obtained from the linear interpolation of the values of GaN and InN.

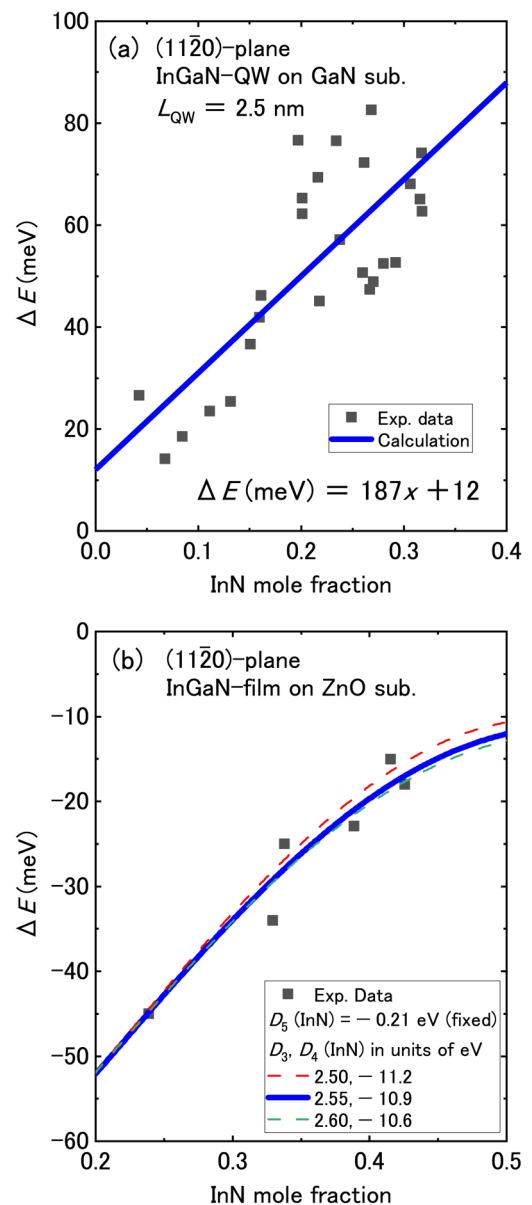
		GaN	InN
Lattice constant (Å)	$a$	3.189 <sup>a</sup>	3.545 <sup>a</sup>
	$c$	5.185 <sup>a</sup>	5.703 <sup>a</sup>
Bandgap at RT (eV)	$E_g$	3.4 <sup>b</sup>	0.65 <sup>b</sup>
Bandgap bowing (eV)	$b$		1.43 <sup>b</sup>
Crystal-field splitting (meV)	$\Delta_1$	12.3 <sup>c</sup>	19 <sup>d</sup>
Spin-orbit interaction (meV)	$\Delta_2$	5.2 <sup>c</sup>	4.3 <sup>d</sup>
	$\Delta_3$	5.9 <sup>c</sup>	4.3 <sup>d</sup>
Electron effective mass	$m_e^{\parallel}$	0.21 <sup>a</sup>	0.07 <sup>a</sup>
	$m_e^{\perp}$	0.20 <sup>a</sup>	0.07 <sup>a</sup>
	$A_1$	-7.21 <sup>a</sup>	-8.21 <sup>a</sup>
	$A_2$	-0.44 <sup>a</sup>	-0.68 <sup>a</sup>
Valence band	$A_3$	6.68 <sup>a</sup>	7.57 <sup>a</sup>
effective mass parameter	$A_4$	-3.46 <sup>a</sup>	-5.23 <sup>a</sup>
	$A_5$	-3.40 <sup>a</sup>	-5.11 <sup>a</sup>
	$A_6$	-4.90 <sup>a</sup>	-5.96 <sup>a</sup>
Conduction band effective	$D_1 - a_{cz}$	6.5 <sup>c</sup>	6.5 <sup>c</sup>
deformation potential (eV)	$D_2 - a_{ct}$	11.2 <sup>c</sup>	11.2 <sup>c</sup>
	$D_3$	4.9 <sup>c</sup>	2.55 <sup>h</sup>
Valence band	$D_4$	-5.0 <sup>c</sup>	-10.9 <sup>h</sup>
deformation potential (eV)	$D_5$	-2.8 <sup>c</sup>	-0.21 <sup>c</sup>
	$D_6$	-3.1 <sup>c</sup>	-13.0 <sup>h</sup>
Elastic constant (GPa)	$c_{11}$	373 <sup>f</sup>	227 <sup>g</sup>
	$c_{12}$	141 <sup>f</sup>	114 <sup>g</sup>
	$c_{13}$	80 <sup>f</sup>	94 <sup>g</sup>
	$c_{33}$	387 <sup>f</sup>	242 <sup>g</sup>
	$c_{44}$	94 <sup>f</sup>	48 <sup>g</sup>

<sup>a</sup>Vurgaftman *et al.*<sup>23</sup><sup>b</sup>Oliva *et al.*<sup>39</sup><sup>c</sup>Ishii *et al.*<sup>17</sup><sup>d</sup>Goldhahn *et al.*<sup>40</sup><sup>e</sup>Mori-Tamamura *et al.*<sup>38</sup><sup>f</sup>Yamaguchi *et al.*<sup>41</sup><sup>g</sup>Peng *et al.*<sup>42</sup><sup>h</sup>This work.

underlying GaN layer and resulting tensile strain along the quantized-axis direction and was calculated according to Hooke's law introducing the rotation matrix.<sup>43</sup> The valence band energy is obtained by diagonalizing the Hamiltonian by introducing the rotation matrix.<sup>44</sup> For simplicity, the calculation was performed as the infinite barrier QW approximation ( $k = \pi/L_{QW}$ ), neglecting internal electric fields.

The used data of energy separation  $\Delta E$  were the  $\Delta E$  of InGaN-QWs with various crystal orientation and InN mole fraction such as (11 $\bar{2}0$ )-plane<sup>45–50</sup> and (11 $\bar{2}2$ )-plane QWs.<sup>14,28–30</sup> InGaN is known for its large potential fluctuations, and optical polarization degree (energy separation  $\Delta E$ ) is dependent on the degree of potential fluctuation and the excited carrier density.<sup>47,51–53</sup> Therefore, even if the InN mole fraction and crystal orientation are the same, the potential fluctuation of InGaN-QW samples and

experimental conditions may differ from one laboratory to another. In this situation, it was difficult to say that this is the correct data. Hence, we collected data on  $\Delta E$  of InGaN-QWs to the best of our knowledge and performed a fitting of the average of the data. From some of references where only emission wavelength and/or optical polarization degree was given, InN mole fraction and  $\Delta E$  were calculated by using single-band Schrödinger equation and

**FIG. 3.** (a) A fitting result for experimental  $\Delta E$  values of  $m(a)$ -plane InGaN-QWs.<sup>45–50</sup> (b) A comparison between the experimental data and the theoretical fitting result for  $\Delta E$  of  $m$ -plane InGaN-film on ZnO substrates.<sup>20</sup>

21 July 2025 08:35:50



Eq. (6) in Ref. 54, respectively. The well width was 2.5 nm, taking the average of the reported values.

Second, we explain the concept for determination of deformation potentials ( $D_3$ – $D_6$ ) in InGaN (InN) by theoretical analysis of experimental data. In our previous study, deformation potential  $D_5$  of InGaN (InN) was determined by applying external uniaxial stress to  $c$ -plane InGaN-QWs.<sup>38</sup> In this experiment, the energy separation is expressed as  $\Delta E \simeq 2D_5(\varepsilon_{xx} - \varepsilon_{yy})$ . Thus, we can obtain only deformation potential  $D_5$  without being affected by other deformation potentials  $D_3$ ,  $D_4$ , and  $D_6$ , and  $D_5$  was estimated as  $-0.21$  eV for InN. Next, in the case for nonpolar ( $m$ - or  $a$ -plane) InGaN-QWs ( $\theta = 90^\circ$ ),  $\Delta E$  is analytically approximated as follows (as  $\Delta_3 = 0$ ):

$$\Delta E = \Delta_1 + \frac{\hbar^2}{2m_0} A_4 \left( \frac{\pi}{L_{\text{QW}}} \right)^2 + D_3 \varepsilon_{zz} + D_4 (\varepsilon_{xx} + \varepsilon_{yy}) + \sqrt{\Delta_2^2 + \left[ -\frac{\hbar^2}{2m_0} A_5 \left( \frac{\pi}{L_{\text{QW}}} \right)^2 + D_5 (\varepsilon_{xx} - \varepsilon_{yy}) \right]^2}. \quad (3)$$

In this equation, since the fitting parameters are  $D_3$  and  $D_4$  giving two degrees of freedom, one more equation is needed in order to remove arbitrariness. Therefore, in addition to the energy separation  $\Delta E$  values for  $m(a)$ -plane InGaN-QWs,<sup>45–50</sup> the values for (1120)-plane InGaN-film on ZnO substrates were also analyzed.<sup>20</sup> By using the difference in strain introduced to InGaN-QWs and

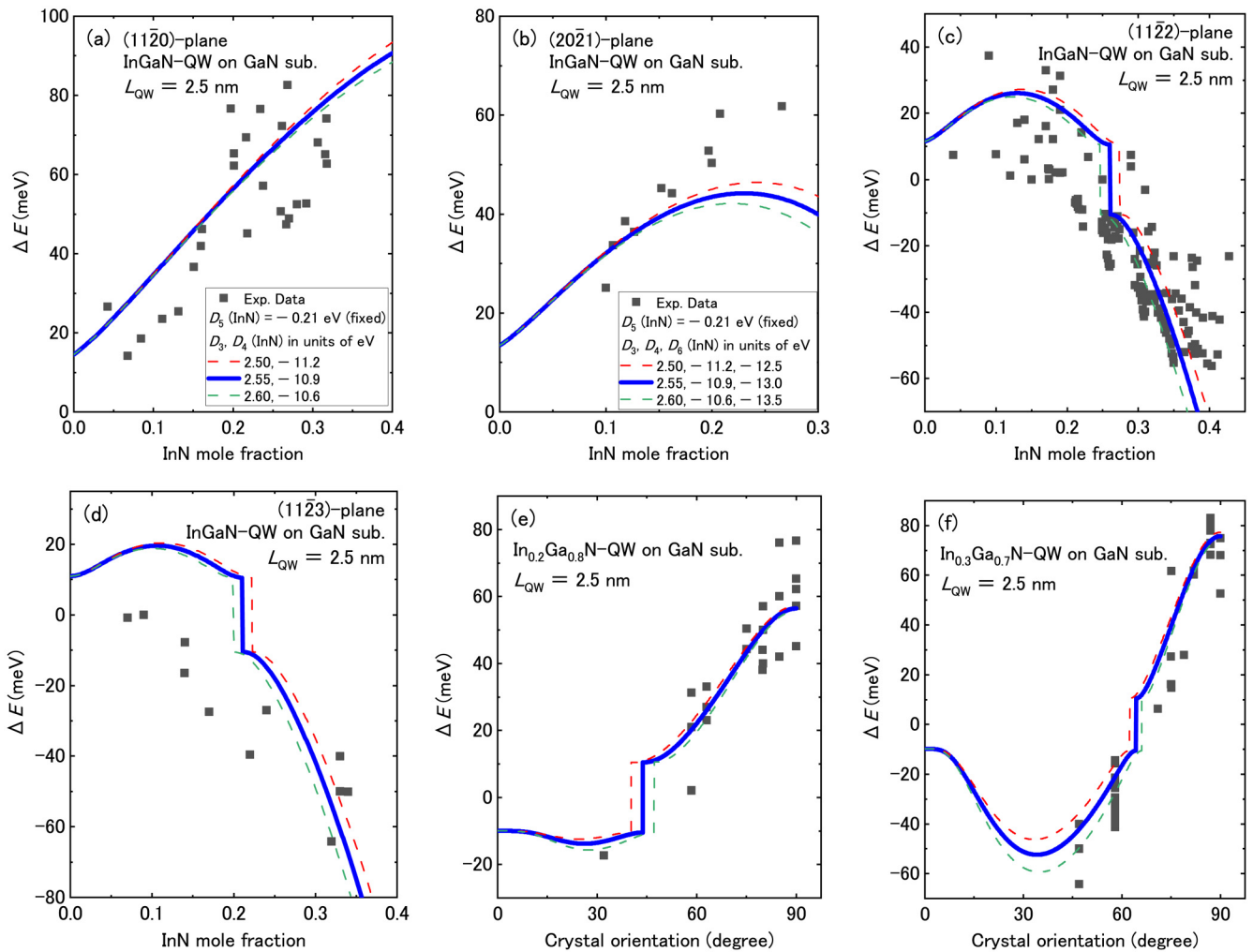


**FIG. 4.** A comparison between the experimental data and the theoretical fitting results for InGaN-QWs with various InN mole fractions and crystal orientations. (a)–(d) InN mole fraction dependence of  $\Delta E$  in non- $c$ -plane InGaN-QW on GaN substrates. (e) and (f) Crystal orientation dependence of  $\Delta E$  in  $\text{In}_{0.2}\text{Ga}_{0.8}\text{N}$ -QW and  $\text{In}_{0.3}\text{Ga}_{0.7}\text{N}$ -QW on GaN substrates. A radical change of  $\Delta E$  in the theoretical curves is caused by the anti-crossing of valence band due to spin-orbit interaction. Red and green dashed lines show respective upper and under errors of theoretical fitting results.

21 July 2025 08:35:50

InGaN-films on GaN and ZnO substrates, respectively, Eq. (3) corresponds to InGaN on GaN and ZnO substrates, respectively, resulting in two equations. Specifically, fitting the experimental values of  $\Delta E$  for (1120)-plane InGaN-QWs with a linear function as shown in Fig. 3(a) and the deformation potential  $D_4$  is expressed as a function of  $D_3$ . Next, substituting this  $D_4$  value into Eq. (3) of calculation for  $\Delta E$  of the  $m$ -plane InGaN-film on ZnO substrates (in this case, QW effect is zero), the theoretical fitting was performed with  $D_3$  as the fitting parameter. Although  $\Delta E$  values of (1120)-plane InGaN-QWs are scattered, we believe the accuracy of the  $\Delta E$  data in the  $m$ -plane InGaN-film on ZnO substrates is high from following reasons. In the case of InGaN on ZnO substrates, the strain of InGaN-films is directly determined by x-ray diffraction measurements, and we used  $\Delta E$  data from pseudo-morphic growth samples. In addition,  $\Delta E$  of InGaN-films on ZnO substrates is not considered to be affected by spectral deconvolution because the data were measured by absorption measurements.<sup>55</sup> Figure 3(b) shows a comparison between the experimental data and the theoretical fitting result for  $\Delta E$  of the  $m$ -plane InGaN-film on ZnO substrates as a function of InN mole fraction. The deformation potentials  $D_3$  and  $D_4$  were simultaneously obtained as  $2.55 \pm 0.05$  and  $-10.9 \pm 0.3$  eV, respectively, for InN by a linear least squares method. Although a discussion of the robustness of obtained  $D_3$  and  $D_4$  values is needed, we could not collect the  $\Delta E$  data of InGaN-QWs at different experimental conditions (such as the data of semipolar InGaN on AlGaIn) to the best of our knowledge.

Finally, the determination of deformation potential  $D_6$  was performed. The used data were all  $\Delta E$  values of InGaN-QWs with various InN mole fraction and crystal orientation except (1120)-plane InGaN-QWs.<sup>14,28–31,45–50,56–63</sup> The method for residual evaluation is as follows. Least squares method (because data points are lacking): InN mole fraction dependence of  $\Delta E$  in (1123)- and (2021)-plane InGaN-QWs. Weighted least squares method: InN mole fraction dependence of  $\Delta E$  in (1122)-plane InGaN-QWs and crystal orientation dependence of  $\Delta E$  in  $\text{In}_{0.2}\text{Ga}_{0.8}\text{N}$ -QWs and  $\text{In}_{0.3}\text{Ga}_{0.7}\text{N}$ -QWs. We calculated the deformation potential for InN  $D_6$  dependence of residual sum of squares for  $\Delta E$  at each InGaN-QW, and a value of  $-13 \pm 0.5$  eV that reproduces the overall experimental value was determined for the deformation potential  $D_6$ . Figure 4 shows a comparison between the experimental data and the theoretical fitting results for InGaN-QWs with various InN mole fraction and crystal orientation. (a)–(d) InN mole fraction dependence of  $\Delta E$  in non- $c$ -plane InGaN-QW on GaN substrates. (e) and (f) Crystal orientation dependence of  $\Delta E$  in  $\text{In}_{0.2}\text{Ga}_{0.8}\text{N}$ -QW and  $\text{In}_{0.3}\text{Ga}_{0.7}\text{N}$ -QW on GaN substrates. In these figures, it is observed that theoretical fitting results almost agree well with experimental data except the results of (2021)-plane and (1123)-plane QWs. However, if the deformation potential  $D_6$  is determined to be  $-8.5$  eV to reproduce the experimental data for the (2021)-plane QWs, the other experimental results do not fit at all. On the other hand, in the case of (1123)-plane QWs, it especially has large discrepancies at low InN mole fraction region ( $0 \leq x \leq 0.2$ ). Thus, it is considered that this is due to the inaccuracy of the material parameters of GaN. The possible reason is valence band effective mass parameters because we used the parameters in Ref. 23 that are derived by using quasi-cubic approximation. Note that the deformation potential values for  $\text{In}_x\text{Ga}_{1-x}\text{N}$  obtained in this study are only

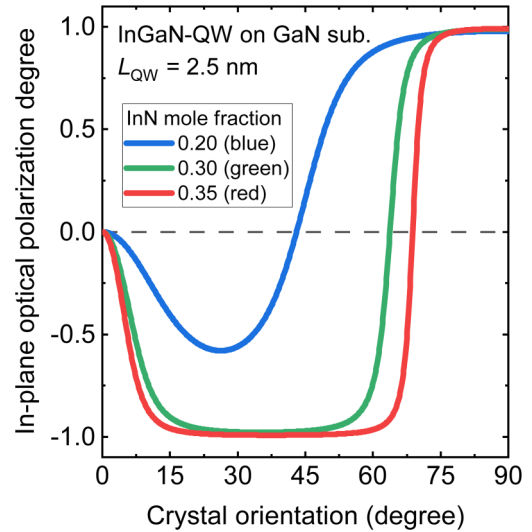


FIG. 5. Crystal orientation dependence of in-plane optical polarization degree of three primary colors emitting InGaN-QWs.

applicable to the visible-emitting region ( $0 \leq x \leq 0.4$ ) because the deformation potentials can be bowing like a bandgap.

The accurate deformation potentials for InGaN that reproduce the experimental data were obtained. We performed a theoretical prediction for realizing blue-, green-, and red-emitting monolithic InGaN-QWs with matching polarization directions. Structure parameters were designed as follows in this theoretical prediction. The InN mole fraction was 0.2, 0.3, and 0.35<sup>64</sup> for blue-, green-, and red-emitting InGaN-QWs, respectively, the well width was 2.5 nm, and substrate was GaN. Figure 5 shows crystal orientation dependence of in-plane optical polarization degree in three primary colors emitting InGaN-QWs. The optical polarization degree was calculated according to Ref. 44. In this figure, the polarization direction is aligned for all emission colors in around (1120)- and (1013)-plane InGaN-QWs. In addition, (1013)-plane InGaN-QWs with negative values of polarization degree can use the cleaved plane for the cavity mirrors in InGaN-based-LDs. The above means that QWs with aligned polarization directions can be grown on the same substrate, which may lead to cost reduction.

### III. CONCLUSION

In summary, we determined the deformation potentials in  $\text{In}_x\text{Ga}_{1-x}\text{N}$  at visible light-emitting region ( $0 \leq x \leq 0.4$ ) based on the  $\mathbf{k} \cdot \mathbf{p}$  perturbation theory. The deformation potentials for InN were obtained as  $D_3 = 2.55$  eV,  $D_4 = -10.9$  eV,  $D_5 = -0.21$  eV, and  $D_6 = -13.0$  eV. In addition, we have performed theoretical calculation for realizing three primary colors emitting InGaN-QWs with matching polarization directions grown on the same substrate and have derived that (1013)-plane QWs can be matched polarization direction emission with usable cleaved plane for cavity mirrors.

21 July 2025 08:35:50

## ACKNOWLEDGMENTS

This work was supported by the Japan Society for the Promotion of Science (JSPS) Grant-in-Aid for Scientific Research (No. JP23K03944).

## AUTHOR DECLARATIONS

## Conflict of Interest

The authors have no conflicts to disclose.

## Author Contributions

**Keito Mori-Tamamura:** Conceptualization (equal); Data curation (equal); Formal analysis (equal); Investigation (equal); Methodology (equal); Visualization (equal); Writing – original draft (equal). **Atsushi A. Yamaguchi:** Funding acquisition (equal); Supervision (equal); Writing – review & editing (equal). **Shuhei Ichikawa:** Supervision (equal); Writing – review & editing (equal). **Kazunobu Kojima:** Project administration (equal); Supervision (equal); Writing – review & editing (equal).

## DATA AVAILABILITY

The data that support the findings of this study are available within the article.

## APPENDIX A: COMPARISON BETWEEN FINITE BARRIER QW WITH INTERNAL ELECTRIC FIELD AND INFINITE BARRIER QW APPROXIMATION WITHOUT INTERNAL ELECTRIC FIELD

We compared results of finite barrier QW with internal electric field and infinite barrier QW approximation without internal

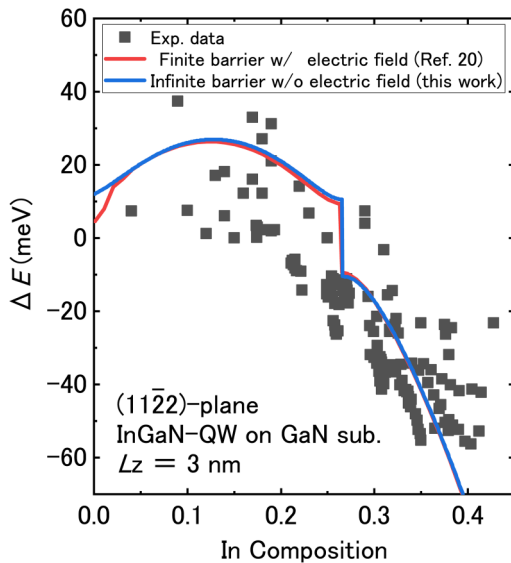


**FIG. 6.** Comparison between finite barrier QW with internal electric field and infinite barrier QW approximation without internal electric field for InN mole fraction dependence of  $\Delta E$  in  $(11\bar{2})$ -InGaN-QWs.

electric field (Fig. 6), in calculation of the  $\Delta E$  in InGaN-QWs based on the  $\mathbf{k} \cdot \mathbf{p}$  perturbation theory. The calculation data under finite barrier QW with internal electric field were obtained from Ref. 21, and the results under infinite barrier QW approximation without internal electric field were calculated by using same material parameters used in this reference. Both calculation results are almost same as shown in this figure, and a difference of both results is considered limitation of energy separation due to band offset at low InN mole fraction region (0–0.03). Therefore, although the calculation using infinite barrier QW approximation without considering internal electric field, we can calculate accurate  $\Delta E$  values of InGaN-QWs.

APPENDIX B: CONNECTION BETWEEN  $\Delta E$  AND POLARIZATION DEGREE

We explain the connection between  $\Delta E$  and optical polarization degree. The optical polarization degree of valence band A ( $\rho$ ) is expressed as follows:<sup>44</sup>

$$\rho = \frac{|M_X^A|^2 - |M_Y^A|^2}{|M_X^A|^2 + |M_Y^A|^2}, \quad (\text{B1})$$

where  $|M_X^A|^2$  and  $|M_Y^A|^2$  are the momentum matrix elements of A-band. The case of polarization degree at RT (assumed to be temperature  $T = 300$  K), we need to consider the hole distribution of the A- and B-bands. Assuming weak excitation region, the hole distribution is considered to follow the Boltzmann distribution. Therefore, the polarization degree at RT expressed ( $\rho_{RT}$ ) as follows:

$$\rho_{RT} \simeq \frac{|M_X^A|^2 - |M_Y^A|^2 + (|M_X^B|^2 - |M_Y^B|^2) \exp\left(-\frac{\Delta E}{k_B T}\right)}{|M_X^A|^2 + |M_Y^A|^2 + (|M_X^B|^2 + |M_Y^B|^2) \exp\left(-\frac{\Delta E}{k_B T}\right)}, \quad (\text{B2})$$

where  $|M_X^B|^2$  and  $|M_Y^B|^2$  are the matrix elements of B-band and  $k_B$  is Boltzmann constant. Because electronic states of A- and B-bands do not have  $|Z, \uparrow\rangle$ -like character, the matrix elements of A- and B-bands are contrasted,

$$|M_X^A|^2 \simeq |M_Y^B|^2, \quad |M_Y^A|^2 \simeq |M_X^B|^2. \quad (\text{B3})$$

Thus, Eq. (B2) becomes

$$\begin{aligned} \rho_{RT} &\simeq \frac{(|M_X^A|^2 - |M_Y^A|^2) \left[1 - \exp\left(-\frac{\Delta E}{k_B T}\right)\right]}{(|M_X^A|^2 + |M_Y^A|^2) \left[1 + \exp\left(-\frac{\Delta E}{k_B T}\right)\right]} \\ &= \rho \frac{1 - \exp\left(-\frac{\Delta E}{k_B T}\right)}{1 + \exp\left(-\frac{\Delta E}{k_B T}\right)}. \end{aligned} \quad (\text{B4})$$

Especially, the absolute value of polarization degree at low temperature is almost unity, Eq. (B4) assumed to be following equation:<sup>54</sup>

$$\Delta E = -k_B T \log\left(\frac{1 - \rho_{RT}}{1 + \rho_{RT}}\right) \leftrightarrow \rho_{RT} = \frac{1 - \exp\left(-\frac{\Delta E}{k_B T}\right)}{1 + \exp\left(-\frac{\Delta E}{k_B T}\right)}. \quad (\text{B5})$$

21 July 2025 08:35:50



## REFERENCES

- <sup>1</sup>Y. Narukawa, M. Ichikawa, D. Sanga, M. Sano, and T. Mukai, *J. Phys. D: Appl. Phys.* **43**, 354002 (2010).
- <sup>2</sup>S. Zhou, Z. Wan, Y. Lei, B. Tang, G. Tao, P. Du, and X. Zhao, *Opt. Lett.* **47**, 1291–1294 (2022).
- <sup>3</sup>D. Iida, P. Kirilenko, M. Velazquez-Rizo, Z. Zhuang, M. A. Najmi, and K. Ohkawa, *AIP Adv.* **12**, 065125 (2022).
- <sup>4</sup>R. Armitage, Z. Ren, M. Holmes, and J. Flemish, *Phys. Status Solidi RRL* **18**, 2400012 (2024).
- <sup>5</sup>T. Takeuchi, S. Sota, M. Katsuragawa, M. Komori, H. Takeuchi, H. A. H. Amano, and I. A. I. Akasaki, *Jpn. J. Appl. Phys.* **36**, L382–L385 (1997).
- <sup>6</sup>T. Takeuchi, C. Wetzel, S. Yamaguchi, H. Sakai, H. Amano, I. Akasaki, Y. Kaneko, S. Nakagawa, Y. Yamaoka, and N. Yamada, *Appl. Phys. Lett.* **73**, 1691–1693 (1998).
- <sup>7</sup>E. Sari, S. Nizamoglu, I.-H. Lee, J.-H. Baek, and H. V. Demir, *Appl. Phys. Lett.* **94**, 211107 (2009).
- <sup>8</sup>T. H. Ngo, B. Gil, B. Damilano, P. Valvin, A. Courville, and P. de Mierry, *J. Appl. Phys.* **122**, 063103 (2017).
- <sup>9</sup>S. Marcinkevičius, R. Yapparov, Y. C. Chow, C. Lynsky, S. Nakamura, S. P. DenBaars, and J. S. Speck, *Appl. Phys. Lett.* **119**, 071102 (2021).
- <sup>10</sup>K. Mori-Tamamura, Y. Morimoto, A. A. Yamaguchi, S. Kusanagi, Y. Kanitani, Y. Kudo, and S. Tomiya, *Jpn. J. Appl. Phys.* **62**, 105501 (2023).
- <sup>11</sup>P. Waltereit, O. Brandt, A. Trampert, H. T. Grahn, J. Menniger, M. Ramsteiner, M. Reiche, and K. H. Ploog, *Nature* **406**, 865–868 (2000).
- <sup>12</sup>M. Ueda, K. Kojima, M. Funato, Y. Kawakami, Y. Narukawa, and T. Mukai, *Appl. Phys. Lett.* **89**, 211907 (2006).
- <sup>13</sup>T. J. Badcock, M. Ali, T. Zhu, M. Pristovsek, R. A. Oliver, and A. J. Shields, *Appl. Phys. Lett.* **109**, 151110 (2016).
- <sup>14</sup>M. Ueda, M. Funato, K. Kojima, Y. Kawakami, Y. Narukawa, and T. Mukai, *Phys. Rev. B* **78**, 233303 (2008).
- <sup>15</sup>A. A. Yamaguchi and K. Kojima, *Phys. Status Solidi C* **9**, 834–837 (2012).
- <sup>16</sup>S.-L. Chuang and C.-S. Chang, *Phys. Rev. B* **54**, 2491–2504 (1996).
- <sup>17</sup>R. Ishii, A. Kaneta, M. Funato, Y. Kawakami, and A. A. Yamaguchi, *Phys. Rev. B* **81**, 155202 (2010).
- <sup>18</sup>B. Gil, M. Moret, O. Briot, S. Ruffenach, C. Giesen, M. Heuken, S. Rushworth, T. Leese, and M. Succi, *J. Cryst. Growth* **311**, 2798–2801 (2009).
- <sup>19</sup>W. G. Scheibenzuber and U. T. Schwarz, *Phys. Status Solidi B* **248**, 647–651 (2011).
- <sup>20</sup>H. Tamaki, A. Kobayashi, J. Ohta, M. Oshima, and H. Fujioka, *Appl. Phys. Lett.* **99**, 061912 (2011).
- <sup>21</sup>S. Sakai, K. Kojima, S. F. Chichibu, and A. A. Yamaguchi, *Jpn. J. Appl. Phys.* **61**, 061003 (2022).
- <sup>22</sup>I. Vurgaftman and J. R. Meyer, *J. Appl. Phys.* **94**, 3675–3696 (2003).
- <sup>23</sup>I. Vurgaftman and J. R. Meyer, “Chapter 2: Electron bandstructure parameters,” in *Nitride Semiconductor Devices: Principles and Simulations*, edited by J. Piprek (Wiley-VCH, 2007), pp. 13–48.
- <sup>24</sup>Q. Yan, P. Rinke, A. Janotti, M. Scheffler, and C. G. V. de Walle, *Phys. Rev. B* **90**, 125118 (2011).
- <sup>25</sup>S. P. Łepkowski, I. Gorczyca, K. Stefańska-Skrobias, N. E. Christensen, and A. Svane, *Phys. Rev. B* **88**, 081202 (2013).
- <sup>26</sup>J. Ziembicki, P. Scharoch, M. P. Polak, M. Wiśniewski, and R. Kudrawiec, *J. Appl. Phys.* **132**, 225701 (2022).
- <sup>27</sup>H. Luo, W. Wu, and S. Lyu, *J. Phys. D: Appl. Phys.* **57**, 145305 (2024).
- <sup>28</sup>H. Masui, H. Asamizu, A. Tyagi, N. F. DeMille, S. Nakamura, and S. P. DenBaars, *Appl. Phys. Express* **2**, 0711002 (2009).
- <sup>29</sup>N. Poyiatzis, J. Bai, R. M. Smith, M. Athanasiou, S. Ghataora, and T. Wang, *Sci. Rep.* **10**, 7191 (2020).
- <sup>30</sup>Y. Tawarazako, N. Nishi, A. Nakata, N. Okada, S. Kurai, Y. Yamada, and K. Tadatomo, *Jpn. J. Appl. Phys.* **62**, SA1019 (2023).
- <sup>31</sup>M. Funato, Y. Matsuda, K. Mori-Tamamura, A. A. Yamaguchi, H. Goto, Y. Sumida, Y. Ishihara, and Y. Kawakami, *J. Appl. Phys.* **131**, 074502 (2022).
- <sup>32</sup>D. J. Dugdale, S. Brand, and R. A. Abram, *Phys. Rev. B* **61**, 12933–12938 (2000).
- <sup>33</sup>P. Rinke, M. Winkelkemper, A. Qteish, D. Bimberg, J. Neugebauer, and M. Scheffler, “Consistent set of band parameters for the group-III nitrides AlN, GaN, and InN based on ab initio calculations,” *Phys. Rev. B* **77**, 075202 (2008).
- <sup>34</sup>A. Punya and W. R. L. Lambrecht, “Electronic structure and band parameters of GaN with dilute b and in alloys,” *Phys. Rev. B* **85**, 195147 (2012).
- <sup>35</sup>J. Wrzesinski and D. Fröhlich, *Phys. Rev. B* **56**, 13087 (1997).
- <sup>36</sup>A. A. Yamaguchi, Y. Mochizuki, C. Sasaoka, A. Kimura, M. Nido, and A. Usui, *Appl. Phys. Lett.* **71**, 374–376 (1997).
- <sup>37</sup>M. Feneberg, J. Däubler, K. Thonke, and R. Sauer, *Phys. Rev. B* **77**, 245207 (2008).
- <sup>38</sup>K. Mori-Tamamura, A. A. Yamaguchi, M. Ohara, T. Makino, R. Koda, and T. Hamaguchi, *Jpn. J. Appl. Phys.* **64**, 031002 (2025).
- <sup>39</sup>R. Oliva, S. J. Zelewski, Ł. Janicki, K. R. Gwóźdź, J. Serafińczuk, M. Rudziński, E. Özbay, and R. Kudrawiec, *Semicond. Sci. Technol.* **33**, 035007 (2018).
- <sup>40</sup>R. Goldhahn, P. Schley, A. T. Winzer, M. Rakel, C. Cobet, N. Esser, H. Lu, and W. J. Schaff, *J. Cryst. Growth* **288**, 273 (2006).
- <sup>41</sup>M. Yamaguchi, T. Yagi, T. Sota, T. Deguchi, K. Shimada, and S. Nakamura, *J. Appl. Phys.* **85**, 8502–8504 (1999).
- <sup>42</sup>H. Peng, Y. X. Han, H. Z. Fu, and X. D. Yang, *J. Alloys Compd.* **475**, 885–888 (2009).
- <sup>43</sup>A. E. Romanov, T. J. Baker, S. Nakamura, and J. S. Speck, *J. Appl. Phys.* **100**, 023522 (2006).
- <sup>44</sup>S.-H. Park and S.-L. Chuang, *Phys. Rev. B* **59**, 4725–4737 (1999).
- <sup>45</sup>S. Nakagawa, H. Tsujimura, K. Okamoto, M. Kubota, and H. Ohta, *Appl. Phys. Lett.* **91**, 171110 (2007).
- <sup>46</sup>M. Kubota, K. Okamoto, T. Tanaka, and H. Ohta, *Appl. Phys. Lett.* **92**, 091120 (2008).
- <sup>47</sup>H. Masui, H. Yamada, K. Iso, S. Nakamura, and S. P. DenBaars, *Appl. Phys. Lett.* **92**, 091105 (2008).
- <sup>48</sup>H. Yamada, K. Iso, M. Saito, H. Masui, K. Fujito, S. P. DenBaars, and S. Nakamura, *Appl. Phys. Express* **1**, 041101 (2008).
- <sup>49</sup>S. You, T. Detchprohm, M. Zhu, W. Hou, E. A. Preble, D. Hanser, T. Paskova, and C. Wetzel, *Appl. Phys. Express* **3**, 102103 (2010).
- <sup>50</sup>D. Kundys, D. Sutherland, M. J. Davies, F. Oehler, J. Griffiths, P. Dawson, M. J. Kappers, C. J. Humphreys, S. Schulz, F. Tang, and R. A. Oliver, *Sci. Tech. Adv. Mater.* **17**, 736–743 (2016).
- <sup>51</sup>D. S. Sizov, R. Bhat, J. Napierala, C. Gallinat, K. Song, and C. Zah, *Appl. Phys. Express* **2**, 071001 (2009).
- <sup>52</sup>K. Kojima, A. A. Yamaguchi, M. Funato, Y. Kawakami, and S. Noda, *Jpn. J. Appl. Phys.* **49**, 081001 (2010).
- <sup>53</sup>N. Poyiatzis, J. Bai, R. M. Smith, M. Athanasiou, S. Ghataora, and T. Wang, *Sci. Rep.* **10**, 7191 (2020).
- <sup>54</sup>K. Kojima, H. Kamon, M. Funato, and Y. Kawakami, *Phys. Status Solidi C* **5**, 3038–3041 (2008).
- <sup>55</sup>S. Sakai, “A study on device characteristics improvement of non-c-oriented InGaN quantum-well light emitters,” Ph.D. thesis (Kanazawa Institute of Technology, 2018).
- <sup>56</sup>R. Sharma, P. M. Pattison, H. Masui, R. M. Farrell, T. J. Baker, B. A. Haskell, F. Wu, S. P. DenBaars, J. S. Speck, and S. Nakamura, *Appl. Phys. Lett.* **87**, 231110 (2005).
- <sup>57</sup>M. Feneberg, F. Lipski, R. Sauer, K. Thonke, P. Brückner, B. Neubert, T. Wunderer, and F. Scholz, *J. Appl. Phys.* **101**, 053530 (2007).
- <sup>58</sup>T. Kyono, Y. Yoshizumi, Y. Enya, M. Adachi, S. Tokuyama, M. Ueno, K. Katayama, and T. Nakamura, *Appl. Phys. Express* **3**, 0110003 (2010).
- <sup>59</sup>R.-B. Chung, Y.-D. Lin, I. Koslow, N. Pfaff, H. Ohta, J. Ha, S. P. DenBaars, and S. Nakamura, *Jpn. J. Appl. Phys.* **49**, 070203 (2010).

<sup>60</sup>Y. Zhao, S. Tanaka, Q. Yan, C.-Y. Huang, R.-B. Chung, C.-C. Pan, K. Fujito, D. Feezell, C. G. V. de Walle, J. S. Speck, S. P. DenBaars, and S. Nakamura, *Appl. Phys. Lett.* **99**, 051109 (2011).

<sup>61</sup>C. Mounir, I. L. Koslow, T. Wernicke, M. Kneissl, L. Y. Kuritzky, N. L. Adamski, S. H. Oh, C. D. Pynn, S. P. DenBaars, S. Nakamura, J. S. Speck, and U. T. Schwarz, *J. Appl. Phys.* **123**, 085705 (2018).

<sup>62</sup>S. Freytag, M. Winkler, R. Goldhahn, T. Wernicke, M. Rychetsky, I. L. Koslow, M. Kneissl, D. V. Dinh, B. Corbett, P. J. Parbrook, and M. Feneberg, *Appl. Phys. Lett.* **116**, 062106 (2020).

<sup>63</sup>Y. Zhao, Q. Yan, D. Feezell, K. Fujito, C. G. V. de Walle, J. S. Speck, S. P. DenBaars, and S. Nakamura, *Opt. Express* **21**, A53 (2013).

<sup>64</sup>D. Iida, Z. Zhuang, P. Kirilenko, M. Velazquez-Rizo, and K. Ohkawa, *Appl. Phys. Express* **13**, 031001 (2020).